water

MDPI

Article

Remote Sensing Estimation of Long-Term Total Suspended Matter Concentration from Landsat across Lake Qinghai

Weibang Li [1], Qian Yang [1,2], Yue Ma [1], Ying Yang [3], Kaishan Song [2], Juan Zhang [4], Zhidan Wen [2] and Ge Liu [2,*]

[1] School of Geomatics and Prospecting Engineering, Jilin Jianzhu University, Changchun 130118, China
[2] Remote Sensing and Geographic Information Research Center, Northeast Institute of Geography and Agroecology, Chinese Academy of Sciences, Changchun 130102, China
[3] Institute of Transportation Development Strategy & Planning of Sichuan Province, Chengdu 610041, China
[4] Field Base Laboratory, Qinghai Institute of Meteorological Science, Xining 810001, China
* Correspondence: liuge@iga.ac.cn; Tel.: +86-181-8683-9506

Abstract: Total suspended matter (TSM) is one of the most widely used water quality parameters, which can influence the light transmission process, planktonic algae, and ecological health. A comprehensive field expedition aiming at water quality assessment was conducted for Lake Qinghai in September 2019. The in-situ measurements were used to support the calibration and validation of TSM concentration using Landsat images. A regional empirical model was established using the top-of-atmosphere (TOA) radiance of Landsat image data at the red band with a wavelength range of 640–670 nm. The coefficient of determination (R^2), mean relative error (MRE), and root mean square error (RMSE) of the TSM estimation model were 0.81, 17.91%, and 0.61 mg/L, respectively. The model was further applied to 87 images during the periods from 1986 to 2020. A significant correlation was found between TSM concentration and daily wind speed ($r = 0.74$, $p < 0.01$, $n = 87$), which revealed the dominance of wind speed on TSM concentration. In addition, hydrological changes also had a significant influence on TSM variations of lake estuaries.

Keywords: Lake Qinghai; Landsat series; total suspended matter; wind

Citation: Li, W.; Yang, Q.; Ma, Y.; Yang, Y.; Song, K.; Zhang, J.; Wen, Z.; Liu, G. Remote Sensing Estimation of Long-Term Total Suspended Matter Concentration from Landsat across Lake Qinghai. *Water* **2022**, *14*, 2498. https://doi.org/10.3390/w14162498

Academic Editor: Thomas Meixner

Received: 19 July 2022
Accepted: 11 August 2022
Published: 13 August 2022

1. Introduction

Lake Qinghai, located in the Qinghai–Tibet Plateau, is the largest inland saltwater lake in China. It functions as a natural barrier for soil and water conservation and desertification control in the inland arid zone of northwest China. It plays a major role in tackling changes in the climate system and maintaining ecological balance [1,2]. With the rapid population growth and socio-economic development, water quality monitoring in Lake Qinghai is essential to achieve better water security and environment management [3]. Among the water quality parameters, suspended particulate matter is an important water quality indicator that can influence light transmission, planktonic algae, and eco-logical health in the lacustrine and riparian environment [4–7]. Suspended particulate matter closely relates to the optical properties and turbidity of water and thereby reflects the underwater light field, especially the depth of light transmission [8,9]. Moreover, suspended particulate matter controls the primary productivity of phytoplankton and hence plays a crucial role in sustaining the aquatic ecosystem [10,11]. Therefore, the monitoring of total suspended matter (TSM) in Lake Qinghai is of great significance for the scientific management of the lake.

The traditional monitoring of suspended matter mainly relies on on-site water sampling through fixed station or ship survey and indoor analysis with high accuracy and reliability. Nevertheless, the large coverage of Lake Qinghai's water bodies requires high tonnage and safety of vessels. The whole-lake survey is time-consuming and labor-intensive, and consumable, high-frequency observation is likely to cause secondary pollution. Limited records of lake-based surveys are available. Some field surveys jointly conducted by the Lanzhou Institute of Geology of the Chinese Academy of Sciences and the Qinghai

Provincial Institute of Biology could be dated back to the 1960s [10,12]. The Southwest University Fishery Resources and Environment Research Centre carried out a lake-wide phytoplankton survey during 2006–2010 [13]. Since 2015, Lake Qinghai National Nature Reserve has been monitoring the water ecology and environment of the lake on an annual basis [14]. Since sampling results are constrained by the representativeness, spatial distribution, and a small number of sampling points, it is difficult to simultaneously present the spatial and temporal distribution characteristics of suspended matter over a large area. To this end, satellite observation offers a powerful alternative for monitoring TSM concentration with the advantage of extensive range, low cost, and high frequency. Despite the monitoring of physical, chemical, and biological parameters across Lake Qinghai in previous studies, the optical properties of its water were not comprehensively investigated using both point-based measurement and pixel-based satellite monitoring.

In general, TSM has been widely monitored by numerous satellite platforms (e.g., ocean color satellite sensors, medium resolution sensors to high-resolution sensors) [6]. The most commonly used satellite sensors include the Sea-viewing Wide Field of view Sensor (SeaWiFS) [15–18], Sentinel-3A Ocean and Land Color Instrument (OLCI) [19], Geostationary Ocean Color Imager (GOCI) [8], SPOT [20,21], Moderate Resolution Imaging Spectroradiometer (MODIS) [22,23], Medium Resolution Imaging Spectrometer (MERIS) [24–27], Landsat series [6,19,28–38], EO-1 Hyperion [39], and so on. Among them, the Landsat series contains four types of sensors: multispectral scanner (MSS), Thematic Mapper (TM), Enhanced Thematic Mapper (ETM+), and Operational Land Imager (OLI). These four sensors provide the longest time series since 1972 and have been the most widely used for TSM derivation due to their relatively high spatial resolution and free accessibility. The reflectance of TSM increases with the bandwidths (from the red to NIR bands), which lays the theoretical foundation for remote sensing. Regarding the low level of TSM of Lake Qinghai, the selection of optimal bands or band combinations along with the bandwidths is needed when inversing TSM and determining turbidity.

Furthermore, the inversion models of TSM mainly consist of semi-empirical/empirical models and semi-analytical/analytical models. An empirical or semi-empirical model relates the corresponding TSM concentration and reflectance data relations based on the band calculation of single-band, multi-band and band ratio, which links the TSM concentration with the actual remote sensing reflectance [40,41]. A semi-analytical/analytical model establishes the relationship between TSM and inherent optical properties (IOPs) based on radiative transfer models [42–45]. For example, the quasi-analytical algorithm (QAA), the most commonly used semi-analytical model, is developed based on the relationship between absorption coefficient, TSM, and remote sensing reflectance [46]. Although semi-analytical/analytical models are more accurate than empirical models under certain conditions, they need more spectral, physical, and chemical parameters of inland water, which limited their wide application. Machine learning methods, such as random forest [9,47] and the neural network [48], require large amounts of data to model and train. It is difficult to sample on a large scale and frequently in Qinghai Lake due to navigation policy. Therefore, previous studies have not implemented a systematic algorithm development and remote sensing investigation of TSM distribution in Lake Qinghai.

To better understand the environmental conditions of Lake Qinghai, the long-term spatial and temporal distribution of TSM is important. To do so, we combined field measurement and remote sensing to monitor the long-term variation of TSM. The objectives of this paper are to (1) develop a reliable inversion model for estimating the TSM of Lake Qinghai from Landsat sensors; (2) analyze the spatial and temporal distribution of TSM during 1986–2020; (3) explore the potential factors affecting TSM concentration in Lake Qinghai based on meteorological and hydrological data.

2. Materials and Methods

2.1. Study Area

Lake Qinghai (99°36′–100°46′ E, 36°32′–37°15′ N) is the largest inland lake in China with an area of about 4500 km^2, as shown in Figure 1 [49,50]. Its mean elevation is about 3200 km, the long shoreline is 455 km with slightly convex shapes, the mean water depth is approximately 20 m, and water volume is roughly 71.6 × 109 m^3 [1,50]. The lake is located at the intersection of the East Asian monsoon zone, the northwest arid zone, and the alpine zone of the Qinghai–Tibet Plateau, with a semi-arid temperate continental climate, regulated by the lake environment and regional climate. Its annual mean temperature ranges from −1.0 to 1.5 °C, annual cumulative precipitation ranges from 300 to 400 mm, evapotranspiration changes from 1300 to 2000 mm, mean wind speed ranges from 3.2 to 4 m/s [51,52]. The catchment area of Lake Qinghai is about 299,660 km^2, and the mean elevation is 3719 m (range: 3036–5053 m). Lake Qinghai is a close lake without outflow [51]. The flows of 48 rivers (watershed area > 5 km^2) entering Lake Qinghai contribute 80% of the water volume of Lake Qinghai. The ice cover duration of Lake Qinghai lasts from December to early April, with a mean ice thickness of about 50 cm and a maximum ice thickness of 70 cm [50,51].

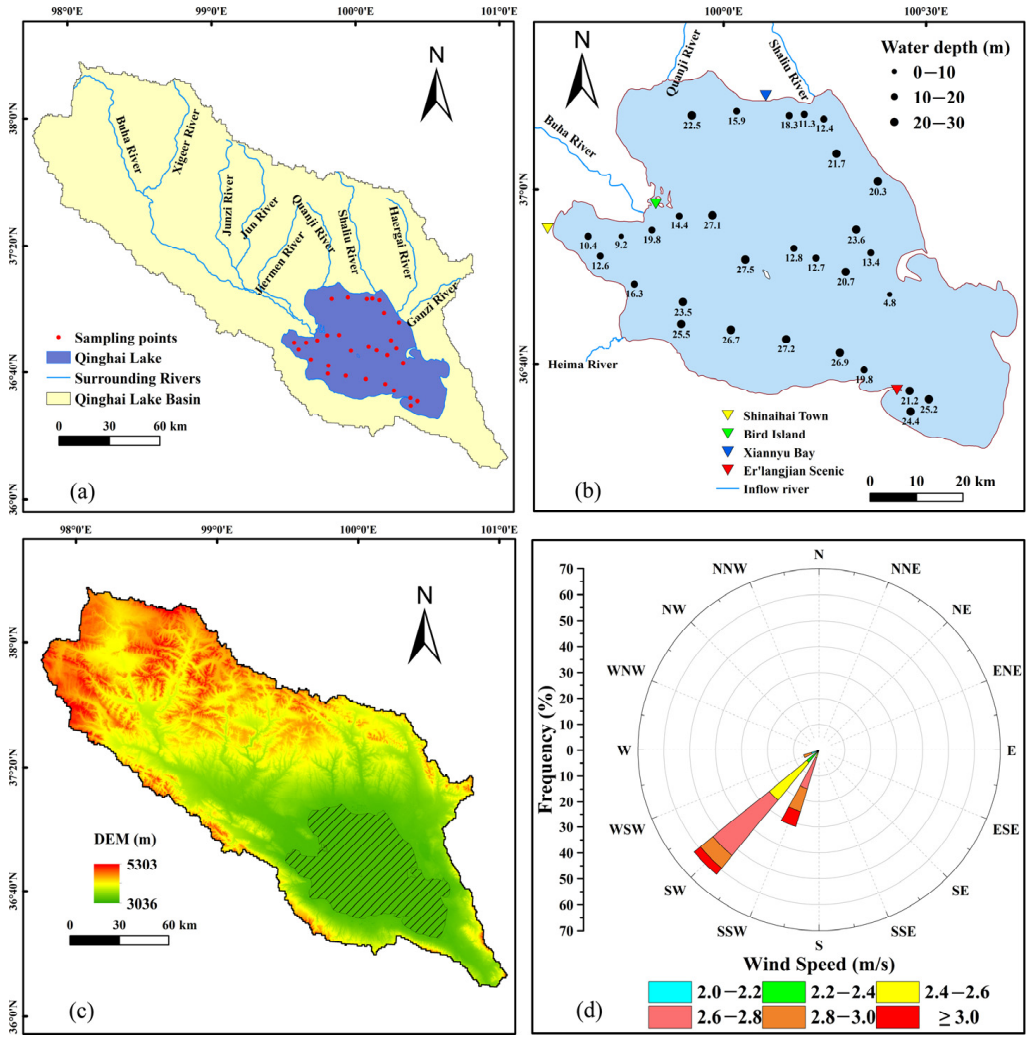

Figure 1. The information of Lake Qinghai and field sampling: (**a**) geographic distribution of Lake Qinghai and the basin; (**b**) spatial distribution of sampling spots and water depth in September 2019; (**c**) the digital elevation map provided by Shuttle Radar Topography Mission (SRTM); (**d**) wind rose of Lake Qinghai.

2.2. Materials

2.2.1. Landsat

The Landsat series was jointly launched by the National Aeronautics and Space Administration (NASA) and the United States Geological Survey (USGS). We used satellite images from three sensors: thematic mapper (TM), enhanced thematic mapper (ETM+), and operational land imager (OLI). Table 1 lists the basic information of these three sensors and the number of images used in this study. The TM, ETM+, and OLI are available for the stages of 1985–2013, 2000–2020, 2013–present. Considering the ice season of Lake Qinghai, the images (with cloud cover <10%) from May to November were selected. Finally, a total of 87 images from 1986 to 2020 were selected with the ranks of 133\34 and 133\35, as shown in Figure 2.

Table 1. The band center of Landsat sensors used in this paper, including thematic mapper (TM), enhanced thematic mapper (ETM+), and operational land imager (OLI).

Band Name	TM/nm	ETM+/nm	OLI/nm
Green band	560	565	562.5
Red band	660	660	655
Image number	33	37	17

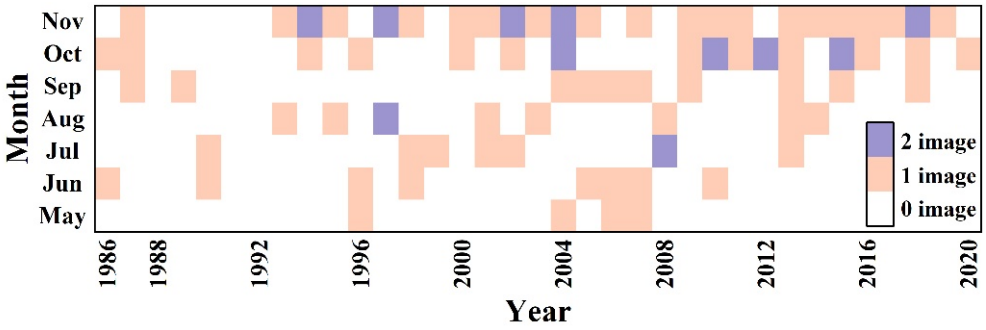

Figure 2. Cloud-free Landsat images of Lake Qinghai used herein during the periods from 1986 to 2020.

2.2.2. Field Measurement

We conducted a field survey on the water environment and water quality in Lake Qinghai basin from 21–22 September 2019. Thirty sampling points were laid out across Lake Qinghai to collect the water samples and the spectra (see our sampling points in Figure 1b). Figure 1b shows the even distribution of sampling points in the central area in Lake Qinghai, away from the estuary, shore, and islands in the lake, where there is a large distribution of water plants. Following Song et al. (2021), the concentrations of TSM of the water samples were measured in the laboratory using the weight method. Besides, we also measured several physical and chemical properties, including water depth (WD), water temperature (WT), the potential of hydrogen (pH), salinity (SAL), dissolved oxygen (DO), total alkalinity (TAI), total nitrogen (TN), total phosphorus (TP), Secchi disc depth (SDD), total suspended matter (TSM), and chlorophyll-a (Chl-a).

We also collected the surface reflectance of the water body using an Analytical Spectral Devices Spectrometer (ASD, Inc., Boulder, CO, USA) FieldSpec 4 under clear weather. Before the measurement, the vessel was anchored to maintain relative stability, and the whiteboard was calibrated. The measurement time was 10:00–14:00 local time (when the solar altitude angle was greater than 45°). The azimuth angle with the sun was kept at 135° and the zenith angle was kept at 45° to avoid the interference of solar flares when measuring. The spectrum acquisition followed this order: reference plate, water surface, sky light, reference plate, and the contribution of the skylight was subtracted from the magnitude of wind speed at the time of measurement when

calculating the water surface remote sensing reflectance. Moreover, at least 10 spectral data were collected at each sampling point. The larger deviation curves were removed, and the remaining values were averaged. Moreover, we also employ the climate and hydrological data of Lake Qinghai from a public dataset provided by National Tibetan Plateau Data Center for further analysis [53].

2.3. Method

Firstly, we determined the sensitive bands for remote sensing inversion by calculating the Pearson correlation coefficients between in-situ spectra and TSM concentration in terms of wavelength. The band with correlation coefficients over 0.75 is considered as the sensitive band. Secondly, we matched the pixel-based reflectance from Landsat images with the indoor-test TSM concentration. Landsat 8 OLI imagery on 24 September 2019 was selected as the modeled remote sensing data, as it was the closest to the field sampling time. The availability of 30 sampling points on Landsat imagery was checked. Among them, 10 sampling points were affected by thin clouds, resulting in anomalous reflectance values. Therefore, the remaining 20 sampling points were divided into two groups: 15 sampling points for modeling and 5 sampling points for validation. Thirdly, linear; power; exponential; logarithmic; and polynomial functions were tested for modeling TSM concentration and reflectance of the single band or band combinations. They were calculated using:

$$TSM = a \times x + b \tag{1}$$

$$TSM = a \times x^2 + b \times x + c \tag{2}$$

$$TSM = a \times x^b \tag{3}$$

$$TSM = a \times \ln(x) + b \tag{4}$$

$$TSM = a \times e^{bx} \tag{5}$$

where a, b, and c are the regression coefficients. The coefficient of determination (R^2), mean relative error (MRE) and root mean square error (RMSE) were used to compare the inversion accuracy of each model and determine the best remote sensing inversion model. They were calculated using:

$$R = \frac{\sum_{i=1}^{n}[(x_i - \overline{x}_i)(y_i - \overline{y}_i)]}{\sqrt{\sum_{i=1}^{n}(x_i - \overline{x}_i)^2\left[\sum_{i=1}^{n}(y_i - \overline{y}_i)^2\right]}} \tag{6}$$

$$R^2 = 1 - \frac{\sum_{i=1}^{n}(y_i - y_i')^2}{\sum_{i=1}^{n}(y_i - \overline{y}_i)^2} \tag{7}$$

$$RMSE = \sqrt{\frac{1}{n}\sum_{i=1}^{n}(y_i - y_i')^2} \tag{8}$$

$$MRE = \sqrt{\frac{\sum_{i=1}^{n} ARE_i^2}{n-2}} \times 100\% \tag{9}$$

where n is the number of samples, x_i is the reflectance of the i sample at a certain wavelength, $\overline{y_i}$ is the mean of all samples, y_i and y_i' are the measured and estimated values for the i sample. The higher the value of R^2, the better the fit; the smaller the value of *MRE*, the higher the reliability; and the smaller the value of *RMSE*, the higher the accuracy of the prediction model in describing the experimental data. After confirming the prediction model with the best performance, the spatial distribution of *TSM* across Lake Qinghai can be mapped during 1986–2021. The time series of yearly and monthly mean values of TSM were also prepared for further analysis.

3. Results

3.1. The Water Quality of Lake Qinghai

Table 2 lists the physical and chemical parameters of Lake Qinghai based on 30 in-situ measurements in September 2019. In general, Lake Qinghai belongs to a brackish water lake because the salinity changed from 10.4 to 11.4‰, with a mean value of 11.1 ± 0.21‰. The water depth ranged (WD) from 4.8 to 27.5 m, with a mean value of 19.1 ± 6.4 m, and the spatial distribution is shown in Figure 1b. A negative correlation between WD and TSM is found with correlation coefficients of 0.48 ($p < 0.01$). The mean values of total nitrogen (TN) and total phosphorus (TP) were 0.58 mg/L and 0.036 mg/L, respectively, which made up the essential nutrients of the lake ecosystem. The dissolved oxygen (DO) varied slightly with a small range of 6.2–6.8 mg/L, suggesting a low concentration of oxygen-consuming pollutants in the water body. The measured TSM ranged from 1.43 to 7.50 mg/L, with a mean value of 3.00 ± 1.48 mg/L. TSM was negatively correlated with Secchi disc depth (SDD) (r = 0.67, $p < 0.01$), both of which indicated the light availability underwater. The chlorophyll-a (Chl-a) concentration was low (ranged from 1.00 to 1.86 μg/L), which was negatively correlated with TSM (r = 0.46, $p < 0.01$). The Chl-a depended on light conditions and rising suspended matter concentrations altered the light intensity, which reduced the phytoplankton productivity and caused the Chl-a content to decline. As suspended matter increased, the absorption and scattering of incident light from the water column also increased, which correlated highly with the transparency of Lake Qinghai. These results indicate the good water quality of Lake Qinghai.

Table 2. The physical and chemical concentrations of Lake Qinghai in September 2019. WD, WT, pH, SAL, DO, TAI, TN, TP, SDD, TSM, and Chl-a, represent water depth, water temperature, potential of hydrogen, salinity, dissolved oxygen, total alkalinity, total nitrogen, total phosphorus, Secchi disc depth, total suspended matter and chlorophyll-a. Min., Max., Mean and SD represent the minimum, maximum, mean value, and standard deviation.

Index	Unit	Min	Max	Mean	SD
WD	meter	4.80	27.50	19.10	6.40
WT	°C	12.90	15.00	14.05	0.48
pH	—	2.10	10.11	8.03	2.68
SAL	‰	10.40	11.40	11.10	0.21
DO	mg/L	6.20	6.80	6.50	0.12
TAI	mg/L	552	612	591	12
TN	mg/L	0.52	0.71	0.58	0.04
TP	mg/L	0.031	0.040	0.036	0.002
SDD	meter	1.80	4.00	3.02	0.62
TSM	mg/L	1.43	7.50	3.00	1.48
Chl-a	μg/L	1.00	1.86	1.43	0.23

3.2. The Inversion Model and the Validation

When using remote sensing products, selecting the optimal and suitable band is the priority for TSM retrieval. Figure 3 shows the reflectance trends of the measured spectra of Lake Qinghai in the wavelength range of 400–900 nm, showing typical spectral characteristics of inland waters with relatively good parallelism [20]. The absorption valleys existed near 450 nm and 600–650 nm, and the reflection peaks existed around 550–600 nm. To further analyze the relationship between remote sensing reflectance and TSM concentration, the change of correlation coefficient between reflectance and TSM concentration at different wavelengths was calculated, as shown in Figure 3b. It is found that the correlation coefficient between reflectance and concentration of Band Green and Band Red exceeded 0.8 for the wavelength range of 570–650 nm, and the correlation was significant. The wavelength range of 570–650 nm was within the coverage of the green (B3) and red (B4) bands of Landsat 8 OLI, so the green (B3) and red (B4) bands were selected as the optimal bands for TSM inversion.

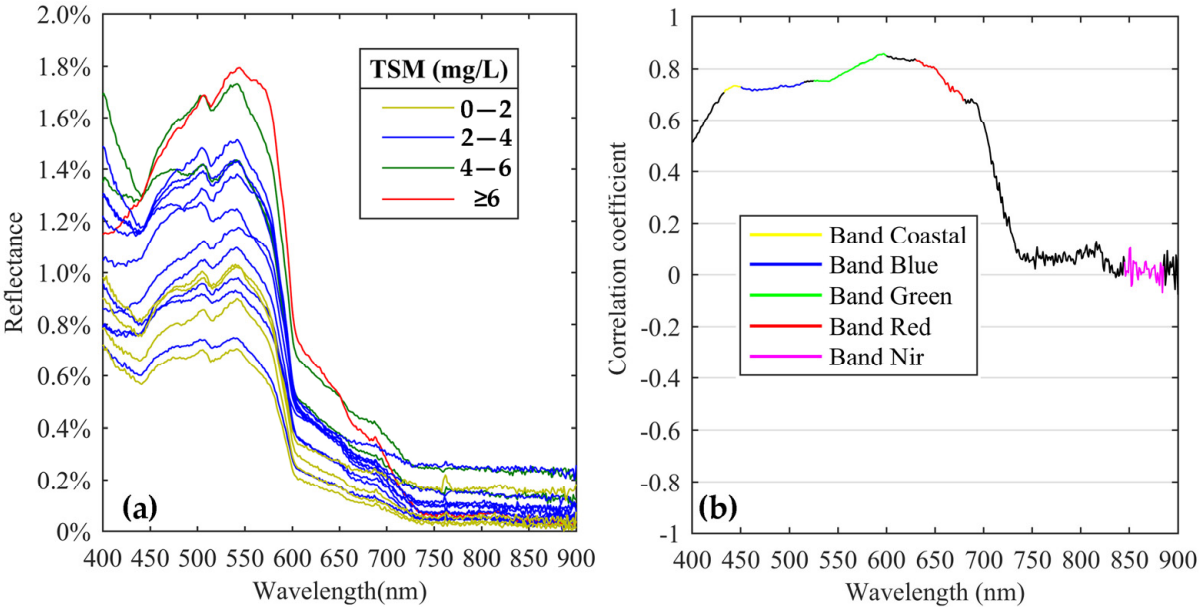

Figure 3. Spectral analysis results: (**a**) reflection spectrum curve of Lake Qinghai; (**b**) correlation coefficient between in-situ reflectance and TSM concentration correction, and different colors correspond to different bands of Landsat 8 OLI sensor.

Figure 4 presents the calibration and validation results of TSM retrieval models (i.e., the linear, power, exponential, logarithmic, and polynomial functions) based on 20 in-situ measurements. Table 3 lists the three assessment indexes for model calibration and validation modeling, including R^2, RMSE, and MRE. We used four band combinations for model construction, including Rrs(Green), Rrs(Red), Rrs(Red)/Rrs(Green), (Rrs(red) + Rrs(Green))/2. To start with, we selected 12 candidates based on the R^2 of model calibration above 0.75 (marked in bold in Table 3). In addition, we picked 4 of 12 models based on the R^2 of model validation above 0.75, including B1, B2, B3, and B5. Considering overfitting, we excluded the B5 model because its R^2 difference (between model calibration and validation) was the largest. The median RMSE of these 11 models (mentioned above) was 0.61, and the RMSEs of B2 and B3 were both greater than 0.61. Therefore, the B1 model established using the red band was finally selected as the optimal model considering the low level of the in-situ TSM across Lake Qinghai, which is expressed as follows:

$$\text{TSM} = 381.97\ \text{Rrs(Red)} - 0.4805 \quad (10)$$

$$R^2 = 0.81,\ \text{RMSE} = 0.61\ \text{mg/L},\ \text{MRE} = 17.91\%$$

3.3. The Water Quality of Lake Qinghai

Figure 5 displays the annual changes in annual average and trends of Landsat-derived TSM data from 1986 to 2020. Overall, the TSM showed *n* downward trend since 1986, which can be grouped into three stages: 1986–2001, 2002–2011, and 2012–2020. The mean TSM from 1986 to 2001 had the highest mean values of 6.22 mg/L and exhibited no trend. From 2002–2011, TSM trended downward, and ranged from 4.6–6.31 mg/L, with a mean value of 5.96 mg/L. From 2012–2020, TSM decreased significantly from 5.98 mg/L to 2.86 mg/L, with a mean value of 3.62 mg/L. Among the three stages, the slope of the linear regression from 2012–2020 was the steepest, indicating a significant drop in TSM from 2012 to 2020.

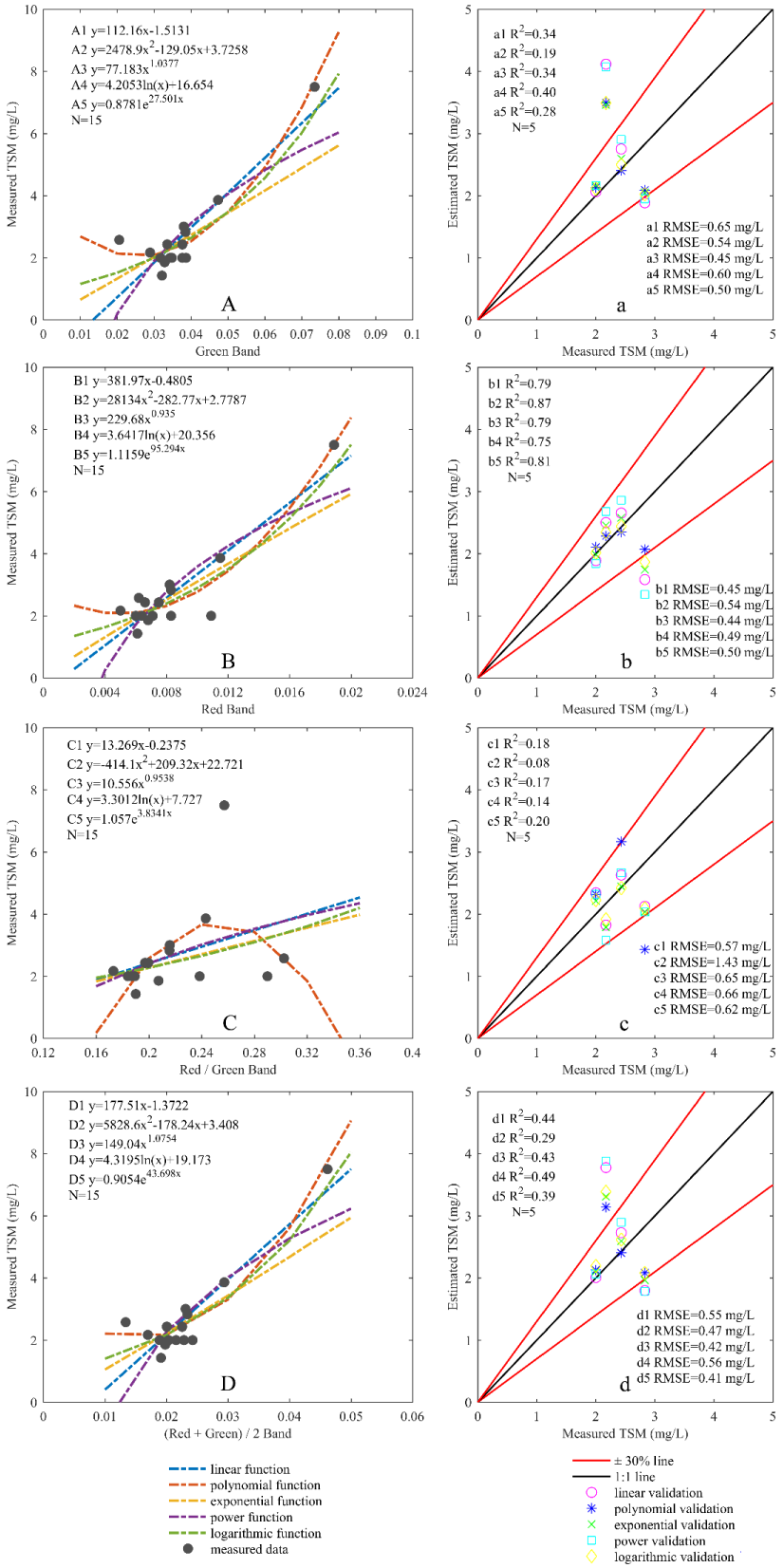

Figure 4. The calibration and validation results of TSM retrieval models are based on 20 in-situ measurements, including linear, power, exponential, logarithmic, and polynomial functions. (**A**–**D**) represent the calibration result of Rrs(Green), Rrs(Red), Rrs(Red)/Rrs (Green), (Rrs(red) + Rrs(Green))/2, and (**a**–**d**) represent the corresponding validation results.

Table 3. The calibration and validation of TSM modeling. A1–D5 and a1–d5 represent different calibration models and validation models in Figure 4. R^2, RMSE, and MRE stand for the coefficient of determination, root mean square error, and mean relative error.

Bands	Calibration Model	R^2	RMSE (mg/L)	MRE (%)	Validation Model	R^2	RMSE (mg/L)	MRE (%)
R_{rs} (Green)	**Figure 3 (A1)**	**0.79**	**0.64**	**28.50**	**Figure 3 (a1)**	**0.34**	**0.65**	**16.21**
	Figure 3 (A2)	**0.92**	**0.39**	**14.10**	**Figure 3 (a2)**	**0.19**	**0.54**	**18.91**
	Figure 3 (A3)	**0.80**	**0.79**	**22.18**	**Figure 3 (a3)**	**0.34**	**0.45**	**15.71**
	Figure 3 (A4)	0.60	0.89	65.52	Figure 3 (a4)	0.40	0.60	13.97
	Figure 3 (A5)	**0.89**	**0.51**	**18.02**	**Figure 3 (a5)**	**0.28**	**0.50**	**17.51**
R_{rs} (Red)	**Figure 3 (B1)**	**0.81**	**0.61**	**17.91**	**Figure 3 (b1)**	**0.79**	**0.45**	**19.06**
	Figure 3 (B2)	**0.89**	**0.66**	**18.30**	**Figure 3 (b2)**	**0.87**	**0.54**	**20.65**
	Figure 3 (B3)	**0.81**	**0.70**	**18.10**	**Figure 3 (b3)**	**0.79**	**0.44**	**17.54**
	Figure 3 (B4)	0.68	0.79	23.50	Figure 3 (b4)	0.75	0.49	20.10
	Figure 3 (B5)	**0.88**	**0.62**	**16.32**	**Figure 3 (b5)**	**0.81**	**0.50**	**19.60**
R_{rs} (Red) /*Rrs* (Green)	Figure 3 (C1)	0.13	1.31	26.64	Figure 3 (c1)	0.18	0.57	23.37
	Figure 3 (C2)	0.29	1.19	26.62	Figure 3 (c2)	0.08	1.43	——
	Figure 3 (C3)	0.13	1.33	28.32	Figure 3 (c3)	0.17	0.65	27.61
	Figure 3 (C4)	0.15	1.30	26.05	Figure 3 (c4)	0.14	0.66	28.24
	Figure 3 (C5)	0.11	1.35	28.92	Figure 3 (c5)	0.20	0.62	25.63
(R_{rs} (Red) + R_{rs}(Green))/2	**Figure 3 (D1)**	**0.82**	**0.60**	**24.06**	**Figure 3 (d1)**	**0.44**	**0.55**	**15.85**
	Figure 3 (D2)	**0.92**	**0.40**	**14.51**	**Figure 3 (d2)**	**0.29**	**0.47**	**17.06**
	Figure 3 (D3)	**0.83**	**0.72**	**20.86**	**Figure 3 (d3)**	**0.43**	**0.42**	**15.28**
	Figure 3 (D4)	0.65	0.83	42.22	Figure 3 (d4)	0.49	0.56	14.48
	Figure 3 (D5)	**0.90**	**0.47**	**16.70**	**Figure 3 (d5)**	**0.39**	**0.41**	**14.63**

Note: 12 candidates for calibration R^2 based on models above 0.75 are shown in bold.

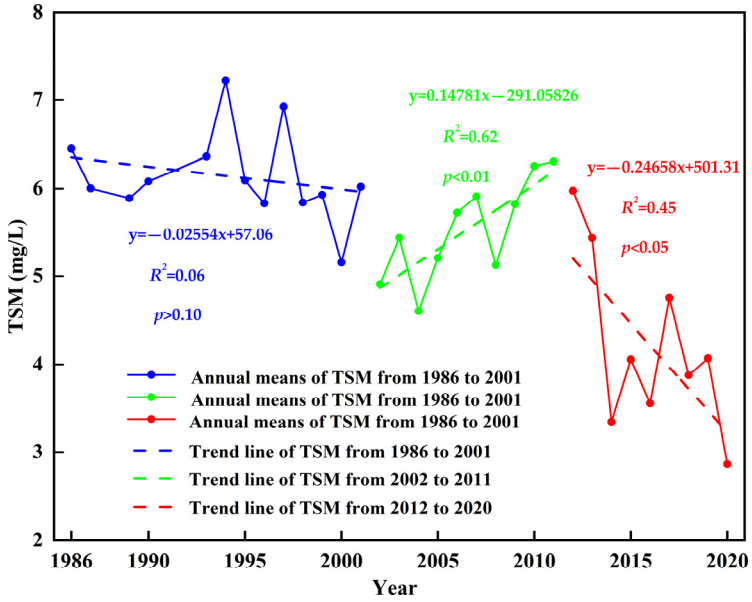

Figure 5. The yearly mean values of TSM across Lake Qinghai since 1986 by averaging all pixels.

Figure 6 displays the spatial distribution of mean TSM for the three stages calculated from the yearly distribution. We used the year average values of all images available from 1986 to 2020 as shown in Figure A1. From 1986 to 2020, the TSM concentration of Lake Qinghai varied widely spatially and temporally. The pixel-based TSM was averaged using all images available within a given year. The spatial gaps in TSM mapping are mainly caused by cloud pixels, and we filtered the abnormal reflectance. Since the revisit cycle of Landsat is 16 days, the ability to monitor the dynamics of TSM is limited. The high TSM concentrations mostly occurred around the estuaries (including Shinaihai Town, Buha, Heima, and Shaliu), while the low TSM concentrations mainly occurred at the lake center.

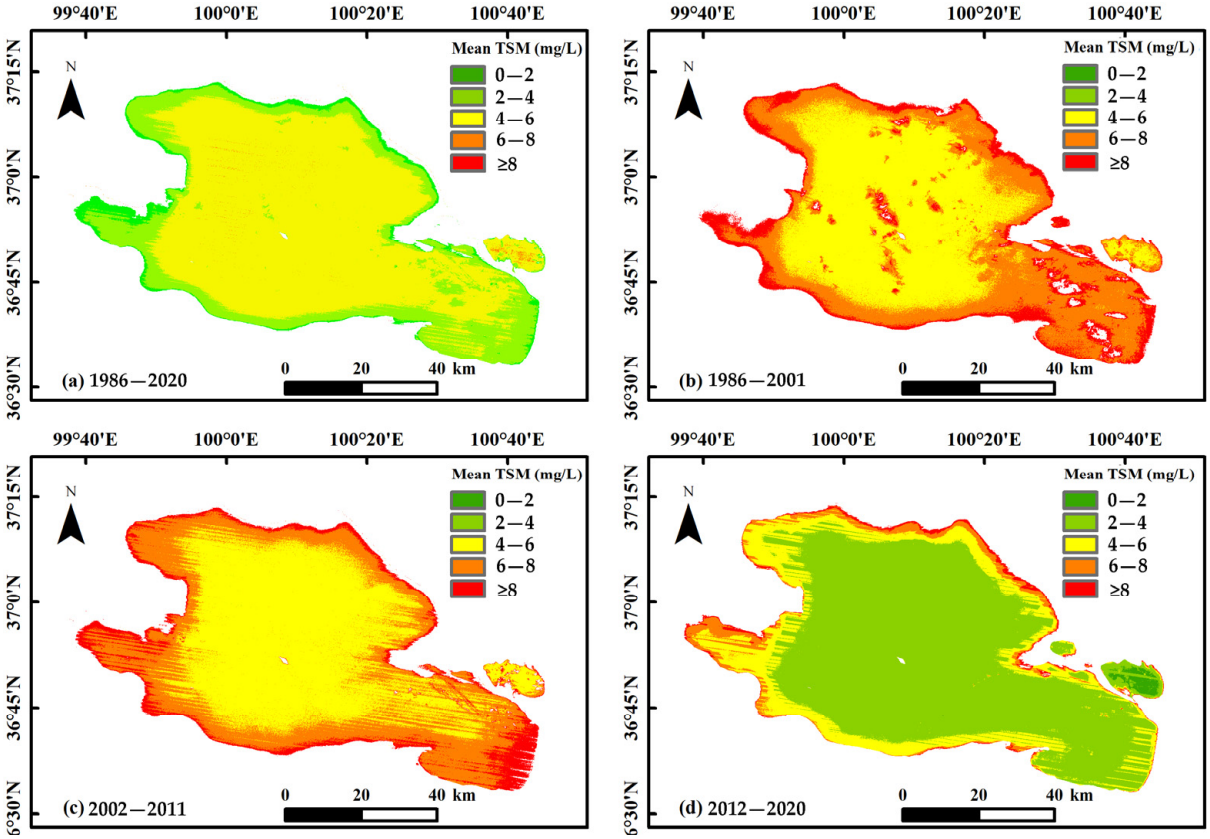

Figure 6. The spatial distribution of mean TSM and changing trend derived from Landsat images during the periods between 1986 to 2020: (**a**) 1986–2020; (**b**) 1986–2001; (**c**) 2002–2011; (**d**) 2012–2020.

We calculated the mean TSM mapping for the three stages, 1986–2001, 2002–2011, and 2012–2020. We classified the TSM concentrations into five groups and the area percentage of each group is shown in Table 4 for the three stages. The mean TSM has been trending downward since 1986. The range of 4–6 mg/L accounted for the largest proportion (>40%) both in 1986–2001 and 2002–2011. For TSM of 2–4 mg/L, the area percentage reached as high as 76.95% in 2012–2020. The percentage of TSM with a range of 4–6 mg/L was the highest in 1986–2001 and 2002–2011, at 48.23% and 65.85%. The percentage of TSM > 6 mg/L was 26.83% and 44.45% below those of 2002–2011 and 1986–2001. For TSM > 8 mg/L, the area percentage has been declining since 1986, which bottomed at 1.7% from 2012 to 2020.

Table 4. The area percentage of different TSM concertation during three periods, including 1986–2001, 2002–2011, and 2012–2020.

Years	Mean TSM	0–2 mg/L	2–4 mg/L	4–6 mg/L	6–8 mg/L	>8 mg/L
1986–2001	6.22 ± 1.35	0.03%	0.02%	48.23%	40.43%	11.29%
2002–2011	5.96 ± 1.22	0.02%	0.03%	65.85%	25.54%	8.56%
2012–2020	3.62 ± 1.32	0.85%	76.95%	14.92%	5.57%	1.70%
1986–2020	5.36 ± 1.23	0.04%	0.39%	71.13%	23.21%	5.23%

Figure 7 illustrates the monthly mean values of TSM across Lake Qinghai since 1986. According to Qi et al. (2020) and Zhang et al. (2021), the mean ice cover duration of Lake Qinghai from December 20 to April 8th during 1986–2021 was 100.11 days. TSM peaked in May, bottomed in June, and then increased again. TSM in August was slightly higher than the adjacent month. Despite the decline of TSM in November, the bottom TSM usually appeared in June. We also calculated the correlation coefficients between yearly TSM averages and meteorological factors (air temperature, precipitation, and wind speed) in terms of yearly and monthly scales (refer to Table 5). Regarding the annual changes, the air

temperature and precipitation correlated negatively with TSM, but the relationship is not significant in the view of seasonal changes. A positive correlation existed between wind speed and TSM on yearly and monthly time scales. Therefore, wind speed played a more important role in TSM changes compared with the other two factors.

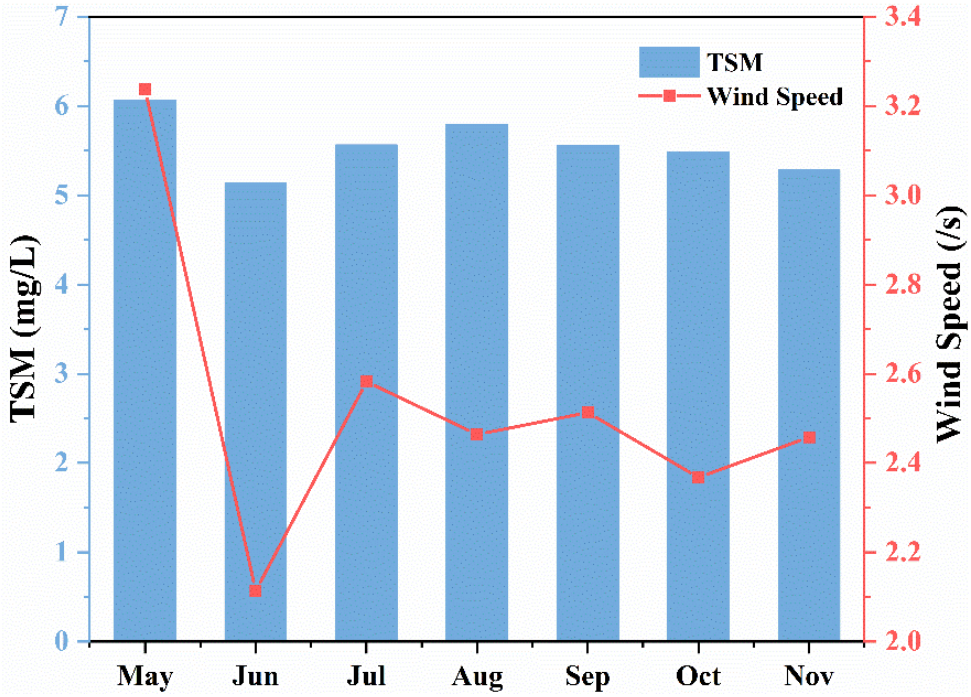

Figure 7. The monthly mean values of TSM across Lake Qinghai from 1986 to 2020.

Table 5. The correlation coefficients between temperature wind speed precipitation and TSM in terms of yearly and monthly scale.

TSM	Air Temperature	Wind Speed	Precipitation
Yearly means	−0.49 **	0.44 *	−0.63 **
Monthly means	0.30	0.86 *	0.47

Note(s): * $p < 0.05$, ** $p < 0.01$.

3.4. The Water Environment of Lake Qinghai

Figure 8 shows the time series of the lake area and lake level of Lake Qinghai since 1986. The lake area and elevation showed a trend from decline to rise, both of which bottomed in 2004. The mean lake area was 4295.28 km^2, with minimum and maximum values of 4205.47 and 4518.95 km^2. The lake level ranged from 3192.86–3196.34 m, with a mean value of 3193.86 m. The lake area of Lake Qinghai has been expanding since 2014, and the lake elevation has become higher. The lake shoreline tended to expand, and the previous grassland for grazing and man-made structure (e.g., parking lot and road) along the shore submerged. The correlation coefficients between lake level and yearly TSM averages was −0.60 ($p < 0.01$), while that between lake area and yearly TSM averages was −0.60 ($p < 0.01$), indicating the crucial role of water extent on TSM changes.

Figure 9 presents the time series of meteorological and hydrological factors of Lake Qinghai since 1986. The wind speed and ice cover duration trended downward, while the precipitation and temperature trended upward. By analyzing the relationship between the influence of each factor on each other, we find that the freezing stage varied most closely with temperature (r = −0.70, $p < 0.01$), which was negatively correlated with the freezing stage. The variations in wind speed and precipitation (r = −0.38, $p < 0.05$) were not significant compared with other factors. This is because the precipitation of Lake Qinghai

was directly affected by temperature (r = 0.41, $p < 0.01$), as reflected in the freezing stage (r = −0.53, $p < 0.01$). The wind speed had some effect on the cloudiness and humidity in the lake area, and the variation in temperature (r = −0.48, $p < 0.01$) was more significant, but it did not directly influence the precipitation.

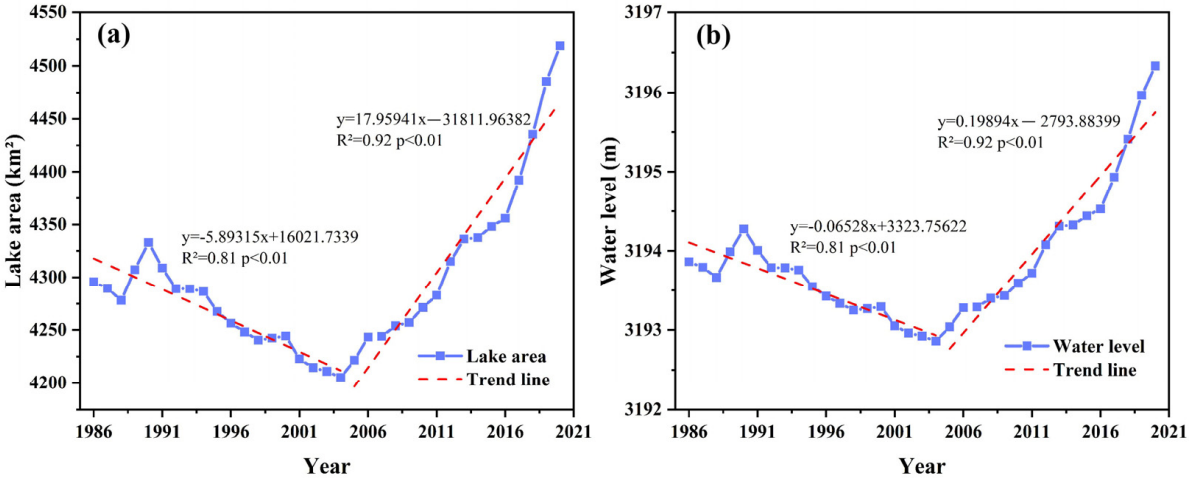

Figure 8. The time series of the lake area and lake level of Lake Qinghai from 1986 to 2020.

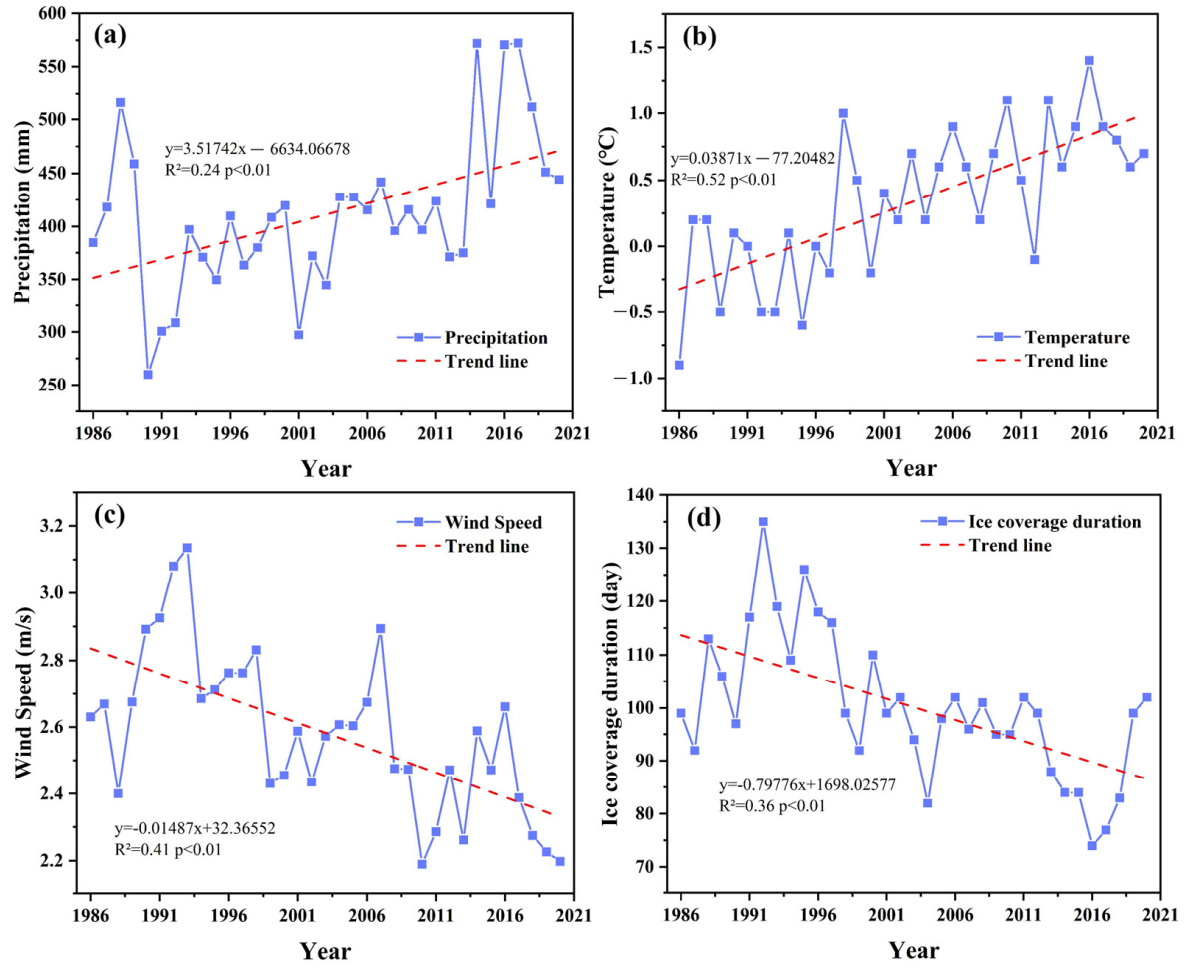

Figure 9. The time series of meteorological and hydrology factors of Lake Qinghai from 1986 to 2020; (**a**) precipitation; (**b**) air temperature; (**c**) wind speed; (**d**) ice cover duration.

Figure 10 shows the spatial changes in shorelines of four estuaries with high TSM values in 1986, 2001, 2004, 2012, and 2020. The images are selected near the annual abundance stage as much as possible, and the band combination is R(7) + G(6) + B(5) of OLI, which can better reduce the interference of cloud cover. Figure 8 suggests that the changes in the water level and water area of Lake Qinghai since 1986 can be roughly divided into two stages, with a downward trend and then an upward trend in the whole time series, reaching the lowest point in 2004. The variation of TSM in Lake Qinghai is closely related to the changes in water level and water area, so four high TSM concentration areas in Lake Qinghai are selected to analyze the shoreline variation by combining the stage nodes of the annual change of TSM of Lake Qinghai. Figure 10 shows that the shoreline change trend in the four high TSM concentration areas is consistent with the changes in water level and water area. It also shows that the shoreline was the farthest away in 2004 and peaked in 2020. Notably, in the standard true color synthetic band, there is a distinctly different image of the water body and land in the expanded area of the Buha River mouth, which might indicate some kind of algae or aquatic plants.

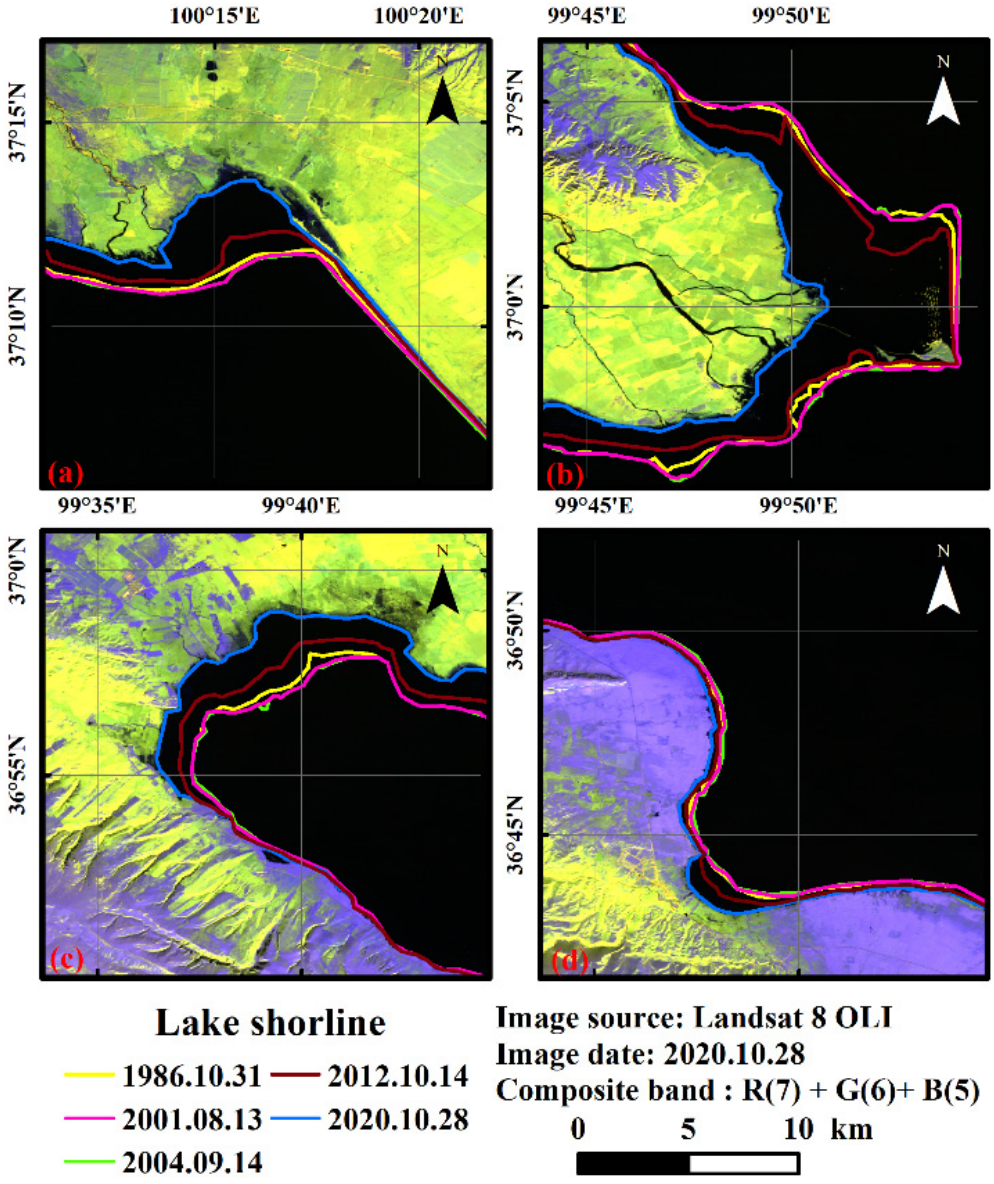

Figure 10. The shorelines of four estuaries of Lake Qinghai in 1986, 2001, 2004, 2012, and 2020. (**a**) Xian'nyu Bay; (**b**) Buha; (**c**) Shinaihai; (**d**) Heima.

4. Discussion

4.1. Model Building

This paper estimated TSM concentrations using three types of Landsat, i.e., TM (stage: 1986–2012), ETM+ (stage: 2000–2012), and OLI (stage: 2013–2018). Ideally, we would build a model for a specific sensor, but the image quality of TM and ETM+ in September 2019 is not qualified for model building with limited field measurements. We also compared the band information of the red band of three Landsat sensors, as shown in Table 2, which are close to each other. The band center of TM, ETM+, and OLI are 660, 660, and 655, respectively. Cao et al. (2019) discussed the effect of bandwidth on water remote sensing (such as PC, TSM, and Chl-a), and suggested the bandwidth for different wavelengths [54], as displayed in Table 3. The best bandwidth for 655–660 nm is 30 nm. The Landsat OLI has narrower bandwidth (30 nm) than the others (60 nm), and it is more reasonable to establish the model and apply to the two remaining sensors. By analyzing the correlation between TSM concentration and measured remote sensing reflectance at different wavelengths, the red and green bands in the range of 570–650 nm were obtained as the optimal band range, which is consistent with the previous research [55–57]. A total of 20 inversion models of five types of functions were developed using a single or a combination of red and green bands. Through model calibration and validation, we developed a red-band based model for TSM inversion with reasonable calibration (R^2 = 0.81, RMSE = 0.61 mg/L, MRE = 17.91%) and validation accuracies (R^2 = 0.79, RMSE = 0.45 mg/L, MRE = 19.06%).

Many mature empirical models [20,56,58–60] and semi-analytical models [46,61,62] have been constructed to estimate TSM concentration for inland lakes. Despite the wide application of red bands in previous studies, there are differences in band combinations and function types. Some studies supplemented them with near-infrared bands in order to obtain better inversion results [58,63], while others anticipated that the ratio model, supplemented with blue-green bands, could better eliminate the influence of yellow substances on TSM concentration [59,64]. The empirical model has a poor spatial expansion and lacks better optical and physical interpretation compared with the analytical model. Although the applications of our model are restricted by sampling location and collection time, the empirical model provides an effective tool to model the long-term spatial and temporal changes of TSM.

4.2. The Change Mode of TSM

In this study, the red band empirical model was applied to 87 Landsat images since 1986. Based on the daily TSM results obtained by inversion, the yearly and monthly TSM conditions from 1986 to 2020 were calculated. The monthly mean TSM in Lake Qinghai was less than 6 mg/L, except for May (6.06 mg/L), and the fluctuation was within 0.93 mg/L. From the field measurements, the mean values of TN and TP were 0.58 mg/L and 0.036 mg/L, respectively, which were much smaller than those of the lakes in southern China [65–68]. Lake Qinghai has good water quality with a relatively low level of TSM [8,60]. Compared with southern lakes, Lake Qinghai is located in the inland area, and the aquatic engineering and human activities are far less, which could explain the small range.

The annual mean TSM showed an obvious three-stage distribution. For the first stage (1986–2001), the overall trend of TSM exhibited little change. During the second stage (2002–2011), TSM significantly trended upward. The tourism industry around Lake Qinghai has been developing vigorously since 2000, but these human activities have affected the environment and ecology due to the lack of overall consideration. The active human activities might explain the rising TSM from 2002 to 2011. In 2007, the Area Protection and Utilization Administration Bureau of Qinghai Province was established with the purpose of achieving better-integrated protection, planning, management, and utilization [69]. After 2012, TSM concentration began to drop, indicating the positive contribution of government policy to the water quality of Lake Qinghai.

From Figure 7, we can see that monthly mean wind speed played an important role in the monthly changes of TSM, and there was a significant positive correlation between wind speed and TSM, which is consistent with the previous study [70,71]. Except for May in spring, TSM from summer (June to August) to autumn (September to November) showed a trend of first increase and then decrease. The accumulated and mean precipitations in summer were 208.91 mm and 69.64 mm, while those in autumn were 54.26 mm and 18.09 mm, respectively. The high precipitation of Lake Qinghai in summer relative to that in autumn might explain the difference in the monthly TSM. Besides, the soil erosion caused by rainfall probably caused the higher turbidity of the lake water and the decrease in transparency [55]. Moreover, precipitation can transport suspended solids from rivers into the lake, leading to an increase in TSM concentration of Lake Qinghai [72].

4.3. Factors Affecting TSM in Lake Qinghai

Lake Qinghai, located inland in northwest China, has a continental plateau climate and a much smaller population density than lakes in southern China. We mainly discussed the influence of meteorological and hydrological factors on TSM. Results showed that TSM was consistent with the trend of ice stage ($r = 0.56$, $p < 0.01$) and wind speed ($r = 0.44$, $p < 0.05$), but contrary to the trend of precipitation ($r = -0.63$, $p < 0.01$) and temperature ($r = -0.49$, $p < 0.01$). Despite a significant correlation between TSM and ice cover, we did not find any direct connection between the environmental conditions of the lake in the non-frozen state. We infer that the significant correlation might be due to the changes in air temperature. The ice cover duration of Lake Qinghai was mainly affected by temperature change ($r = -0.71$, $p < 0.01$). Temperature change has a certain effect on TSM, and the molecule moves faster in a high-temperature environment, which increases the disturbance of suspended matter in the lake. However, our results suggested a negative correlation between TSM and temperature. By further analyzing the correlation between TSM and lake surface temperature, we found that the correlation was insignificant ($r = -0.20$, $p > 0.1$). The influence of water temperature and air temperature on TSM is not clear. As a result, we did not find much obvious effect of ice cover duration and temperature on TSM changes.

Furthermore, the air temperature played an obvious role in precipitation ($r = -0.41$, $p < 0.01$). According to Cheng et al. and Zhang et al. [73,74], the increase in temperature would increase evaporation and water vapor content in the atmosphere, causing an increase in precipitation. Precipitation and wind speed have been identified as the major factors [9,75] affecting TSM in inland lakes. A certain wind speed would interfere with the distribution of suspended matter in the lake, resulting in suspended matter re-suspension [70,71]. We also matched daily TSM and wind speed in Lake Qinghai and obtained a more significant correlation ($r = 0.74$, $p < 0.01$), which corresponded to the monthly and yearly results.

The changes in the water level and water area of Lake Qinghai can influence TSM in a complex manner. The water level and water area of Lake Qinghai firstly decreased and then increased from 1986 to 2020, which agrees with the previous work [53]. Hydrological changes influence significantly the water quality and environment of lake estuaries [76]. The rising water level and expanding water coverage flooded the original pasture, where the herdsmen graze and live, and created a newly flooded area. The original vegetation and grazing excrement would be quickly released into the water in a short time, which is distributed along the estuaries with high TSM concentrations. For example, the bird island area on the west bank of Lake Qinghai has experienced the largest changes in shoreline in the neighborhood of the Buha River in Figure 10. The humus of plant residues in submerged pasture and grassland would increase the TSM content in the lake and provide conditions for lake algae to epiphytic entangling, which would in turn endanger bird breeding [77]. However, higher water levels and water areas are also important indications of the improvement of the ecological environment in Lake Qinghai. During the second stage (2002–2011), TSM in Lake Qinghai was negatively affected by the increase in water level and water area and showed a slight upward trend

(k = 0.15, R^2 = 0.62, $p < 0.01$), while in the third stage (2012–2020), it was the opposite. More generally, in the long term, the water quality of Lake Qinghai is improving with decreasing TSM concentrations.

5. Conclusions

In this paper, for the first time, we combined in-situ measurements and remote sensing images to rigorously investigate the 35-year spatial and temporal changes of TSM in Lake Qinghai. The red spectra-based model performed well for TSM retrieval with R^2, RMSE, and MRE of 0.81, 0.61 mg/L, and 17.91%, respectively, which is further applied to 87 Landsat images. From the long-term stage of 1986–2020, the trend of TSM exhibited a decreasing trend and has been grouped into three stages: 1986–2001, 2002–2011, and 2012–2020, which is closely associated with the environment conservation of Lake Qinghai. In terms of spatial distribution, the TSM concentrations showed low concentrations in the lake center and high concentrations around the water boundaries, especially for the estuaries (e.g., Buha, Heima, and Shaliu). The rising water level and expanding water extent since 2004 flooded the original pasture and exposed the original vegetation and grazing excrement, which explained the high concentrations of TSM in the estuaries. We also compared the correlation between TSM and air temperature, precipitation, wind speed, and ice cover duration. Our results suggested that precipitation and wind speed played a more crucial role on TSM in view of season changes. Although this study can provide a theoretical basis and technical support for large-scale and rapid inversion of the suspended concentrations in Lake Qinghai, the effects of inherent optical parameters (e.g., yellow matter, suspended matter composition, and particle size) on suspended matter concentrations should be considered in future studies.

Author Contributions: Conceptualization, W.L. and Q.Y.; methodology, Q.Y. and Y.Y.; software, W.L. and G.L.; validation, J.Z.; investigation Y.Y.; formal analysis, Y.M. and Z.W.; writing—original draft preparation, Q.Y. and W.L.; writing—review and editing, Q.Y., K.S. and W.L.; funding acquisition, Z.W. and K.S. All authors have read and agreed to the published version of the manuscript.

Funding: This research was jointly supported by the National Key Research and Development Program of China (No. 2021YFB3901101), the National Natural Science Foundation of China (42171374, 42071336, 42171385), and National Tibetan Plateau Data Center (http://data.tpdc.ac.cn, accessed on 21 May 2022).

Institutional Review Board Statement: Not applicable.

Informed Consent Statement: Not applicable.

Data Availability Statement: The datasets used and analyzed during the current study are available from the corresponding authors upon reasonable request.

Acknowledgments: The authors would like to gratefully acknowledge the USGS for providing Landsat images and thank National Tibetan Plateau Data Center for climate and hydrological data. The anonymous reviewers to improve the quality of this manuscript are greatly appreciated.

Conflicts of Interest: The authors declare no conflict of interest.

Appendix A

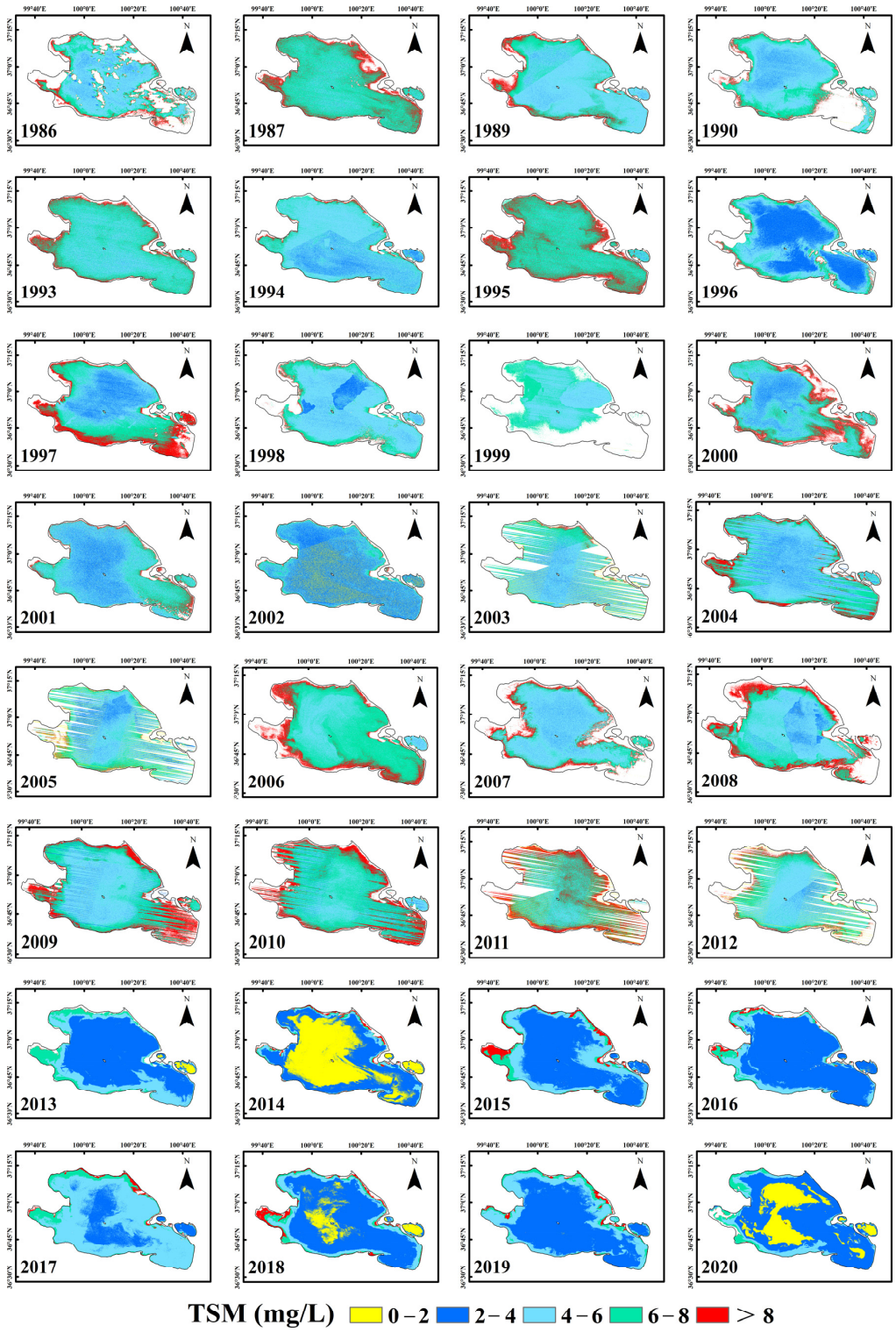

Figure A1. The spatial distribution of TSM of Lake Qinghai from 1986 and 2020 using Landsat sensors, including ETM+, TM, and OLI. We used the year average values of all images available within a given year.

References

1. Han, W.; Huang, C.; Gu, J.; Hou, J.; Zhang, Y. Spatial-Temporal Distribution of the Freeze–Thaw Cycle of the Largest Lake (Qinghai Lake) in China Based on Machine Learning and MODIS from 2000 to 2020. *Remote Sens.* **2021**, *13*, 1695. [CrossRef]
2. Liu, Y.; Chen, H.; Wang, H.; Sun, J.; Li, H.; Qiu, Y. Modulation of the Kara Sea Ice Variation on the Ice Freeze-Up Time in Lake Qinghai. *J. Clim.* **2019**, *32*, 2553–2568. [CrossRef]
3. Pulliainen, J.; Kallio, K.; Eloheimo, K.; Koponen, S.; Servomaa, H.; Hannonen, T.; Tauriainen, S.; Hallikainen, M. A semi-operative approach to lake water quality retrieval from remote sensing data. *Sci. Total Environ.* **2001**, *268*, 79–93. [CrossRef]
4. Dekker, A.; Vos, R.; Peters, S. Comparison of remote sensing data, model results and in situ data for total suspended matter (TSM) in the southern Frisian lakes. *Sci. Total Environ.* **2001**, *268*, 197–214. [CrossRef]
5. Du, Y.; Song, K.; Liu, G.; Wen, Z.; Fang, C.; Shang, Y.; Zhao, F.; Wang, Q.; Du, J.; Zhang, B. Quantifying total suspended matter (TSM) in waters using Landsat images during 1984–2018 across the Songnen Plain, Northeast China. *J. Environ. Manag.* **2020**, *262*, 110334. [CrossRef]
6. Lymburner, L.; Botha, E.; Hestir, E.; Anstee, J.; Sagar, S.; Dekker, A.; Malthus, T. Landsat 8: Providing continuity and increased precision for measuring multi-decadal time series of total suspended matter. *Remote Sens. Environ.* **2016**, *185*, 108–118. [CrossRef]
7. Song, K.; Li, L.; Wang, Z.; Liu, D.; Zhang, B.; Xu, J.; Du, J.; Li, L.; Li, S.; Wang, Y. Retrieval of total suspended matter (TSM) and chlorophyll-a (Chl-a) concentration from remote-sensing data for drinking water resources. *Environ. Monit. Assess.* **2012**, *184*, 1449–1470. [CrossRef]
8. Lei, S.; Xu, J.; Li, Y.; Du, C.; Liu, G.; Zheng, Z.; Xu, Y.; Lyu, H.; Mu, M.; Miao, S.; et al. An approach for retrieval of horizontal and vertical distribution of total suspended matter concentration from GOCI data over Lake Hongze. *Sci. Total Environ.* **2019**, *700*, 134524. [CrossRef]
9. Wang, X.; Wen, Z.; Liu, G.; Tao, H.; Song, K. Remote estimates of total suspended matter in China's main estuaries using Landsat images and a weight random forest model. *ISPRS J. Photogramm. Remote Sens.* **2021**, *183*, 94–110. [CrossRef]
10. Du, J.; Li, Q.; Liu, X.; Wen, D. Hydrological characteristics of Qinghai Lake, 1956–2017. *J. Hydroecol.* **2020**, *41*, 27–33. [CrossRef]
11. Xue, K.; Ma, R.; Shen, M.; Li, Y.; Duan, H.; Cao, Z.; Wang, D.; Xiong, J. Variations of suspended particulate concentration and composition in Chinese lakes observed from Sentinel-3A OLCI images. *Sci. Total Environ.* **2020**, *721*, 137774. [CrossRef] [PubMed]
12. Northwest Institute of Plateau Biology; Chinese Academy of Sciences. *Studies on Biology of Fish fauna and Gymnocypris przewalskii in Qinghai Lake*; Beijing Science Press: Beijing, China, 1975. (In Chinese)
13. Yao, W.Z.; Shi, J.Q.; Qi, H.F.; Yang, J.X.; Jia, S.; Pu, J.; Northwest Institute of Plateau Biology; Chinese Academy of Sciences. Studies on biology of *Fish fauna* and *Gymnocypris przewalskii* in Qinghai Lake. *Freshw. Fish.* **2011**, *41*, 7. (In Chinese).
14. Bi, R.; Zhang, H.; Li, H.; Chang, F.; Duan, L.; He, Y.; Zhang, H.; Wen, X.; Zhou, Y. Characteristics and Changes of Water Quality Parameters of Qinghai Lake in 2015. *J. Water Resour. Res.* **2018**, *7*, 74–83. (In Chinese) [CrossRef]
15. D'Sa, E. Colored dissolved organic matter in coastal waters influenced by the Atchafalaya River, USA: Effects of an algal bloom. *J. Appl. Remote Sens.* **2008**, *2*, 183–198. [CrossRef]
16. Kahru, M.; Mitchell, B.G. Seasonal and nonseasonal variability of satellite-derived chlorophyll and colored dissolved organic matter concentration in the California Current. *J. Geophys. Res. Earth Surf.* **2001**, *106*, 2517–2529. [CrossRef]
17. O'Reilly, J.E.; Maritorena, S.; Mitchell, B.G.; Siegel, D.A.; Carder, K.L.; Garver, S.A.; Kahru, M.; McClain, C. Ocean color chlorophyll algorithms for SeaWiFS. *J. Geophys. Res.-Ocean.* **1998**, *103*, 24937–24953. [CrossRef]
18. Siegel, D.A.; Maritorena, S.; Nelson, N.B.; Hansell, D.A.; Lorenzi-Kayser, M. Global distribution and dynamics of colored dissolved and detrital organic materials. *J. Geophys. Res.-Ocean.* **2002**, *107*, 21. [CrossRef]
19. Huovinen, P.; Ramírez, J.; Caputo, L.; Gómez, I. Mapping of spatial and temporal variation of water characteristics through satellite remote sensing in Lake Panguipulli, Chile. *Sci. Total Environ.* **2019**, *679*, 196–208. [CrossRef]
20. Doxaran, D.; Froidefond, J.-M.; Lavender, S.; Castaing, P. Spectral signature of highly turbid waters. *Remote Sens. Environ.* **2002**, *81*, 149–161. [CrossRef]
21. Goodin, U.G.; Harrington, J.A.; Nellis, M.D.; Rundquist, D.C. Mapping Reservoir Turbidity Patterns Using SPOT-HRV Data. *Geocarto Int.* **1996**, *11*, 71–78. [CrossRef]
22. Chen, Z.; Muller-Karger, F.E.; Hu, C. Remote sensing of water clarity in Tampa Bay. *Remote Sens. Environ.* **2007**, *109*, 249–259. [CrossRef]
23. Feng, L.; Hu, C.; Chen, X.; Tian, L.; Chen, L. Human induced turbidity changes in Poyang Lake between 2000 and 2010: Observations from MODIS. *J. Geophys. Res. Ocean.* **2012**, *117*, 1–19. [CrossRef]
24. Juhls, B.; Overduin, P.P.; Hlemann, J.; Hieronymi, M.; Fischer, J. Dissolved Organic Matter at the Fluvial-Marine Transition in the Laptev Sea Using in situ Data and Ocean Color Remote Sensing. *Biogeosciences* **2019**, *16*, 2693–2713. [CrossRef]
25. Koponen, S.; Pullainen, J.; Kallio, K.; Hallikainen, M. Lake water quality classification with airborne hyperspectral spectrometer and simulated MERIS data. *Remote Sens. Environ.* **2002**, *79*, 51–59. [CrossRef]
26. Ouillon, S.; Douillet, P.; Petrenko, A.; Neveux, J.; Dupouy, C.; Froidefond, J.-M.; Andréfouët, S.; Muñoz-Caravaca, A. Optical Algorithms at Satellite Wavelengths for Total Suspended Matter in Tropical Coastal Waters. *Sensors* **2008**, *8*, 4165–4185. [CrossRef]
27. Zhang, Y.; Shi, K.; Liu, X.; Zhou, Y.; Qin, B. Lake Topography and Wind Waves Determining Seasonal-Spatial Dynamics of Total Suspended Matter in Turbid Lake Taihu, China: Assessment Using Long-Term High-Resolution MERIS Data. *PLoS ONE* **2014**, *9*, e98055. [CrossRef]

28. Bustamante, J.; Pacios, F.; Díaz-Delgado, R.; Aragonés, D. Predictive models of turbidity and water depth in the Doñana marshes using Landsat TM and ETM+ images. *J. Environ. Manag.* **2009**, *90*, 2219–2225. [CrossRef]
29. Braga, C.Z.F.; Setzer, A.W.; Lacerda, L. Water quality assessment with simultaneous Landsat-5 TM data at Guanabara Bay, Rio de Janeiro, Brazil. *Remote Sens. Environ.* **1993**, *45*, 95–106. [CrossRef]
30. Alparslan, E.; Coskun, H.G.; Alganci, U. Water Quality Determination of Küçükçekmece Lake, Turkey by Using Multispectral Satellite Data. *Sci. World J.* **2015**, *9*, 1215–1229. [CrossRef]
31. Gan, T.Y.; Kalinga, O.A.; Ohgushi, K.; Araki, H. Retrieving seawater turbidity from Landsat TM data by regressions and an artificial neural network. *Int. J. Remote Sens.* **2004**, *25*, 4593–4615. [CrossRef]
32. Gao, F.; Wang, Y.; Hu, X. Evaluation of the suitability of Landsat, MERIS, and MODIS for identifying spatial distribution patterns of total suspended matter from a self-organizing map (SOM) perspective. *Catena* **2019**, *172*, 699–710. [CrossRef]
33. Lathrop, R.G. Landsat Thematic Mapper Monitoring of Turbid Inland Water Quality. *Photogramm. Eng. Remote Sens.* **1992**, *58*, 229–250. [CrossRef]
34. Lathrop, R.G.; Lillesand, T.M. Use of Thematic Mapper Data to Assess Water Quality in Green Bay and Central Lake Michigan. *Photogramm. Eng. Remote Sens.* **1986**, *52*, 10–15.
35. Cai, L.; Yu, W.; Shao, W.; Tang, D.; Belkin, I.M. Satellite observations of suspended sediment near Ningbo North Dyke, China. *Adv. Space Res.* **2019**, *64*, 1415–1422. [CrossRef]
36. Peterson, K.T.; Sagan, V.; Sidike, P.; Cox, A.L.; Martinez, M. Suspended Sediment Concentration Estimation from Landsat Imagery along the Lower Missouri and Middle Mississippi Rivers Using an Extreme Learning Machine. *Remote Sens.* **2018**, *10*, 1503. [CrossRef]
37. Ritchie, J.C.; Schiebe, F.R.; Mchenry, J.R. Remote Sensing of Suspended Sediments in Surface Water. *Photogramm. Eng. Remote Sens.* **1976**, *42*, 1539–1545.
38. Wang, H.; Yang, Z.; Saito, Y.; Liu, J.P.; Sun, X. Interannual and seasonal variation of the Huanghe (Yellow River) water discharge over the past 50 years: Connections to impacts from ENSO events and dams. *Glob. Planet. Chang.* **2006**, *50*, 212–225. [CrossRef]
39. Brando, V.E.; Dekker, A.G. Satellite Hyperspectral Remote Sensing for Estimating Estuarine and Coastal Water Quality. *IEEE Trans. Geosci. Remote Sens.* **2003**, *41*, 1378–1387. [CrossRef]
40. Cao, Z.; Duan, H.; Feng, L.; Ma, R.; Xue, K. Climate- and human-induced changes in suspended particulate matter over Lake Hongze on short and long timescales. *Remote Sens. Environ.* **2017**, *192*, 98–113. [CrossRef]
41. Ondrusek, M.; Stengel, E.; Kinkade, C.; Vogel, R.; Keegstra, P.; Hunter, C.; Kim, C. The development of a new optical total suspended matter algorithm for the Chesapeake Bay. *Remote Sens. Environ.* **2012**, *119*, 243–254. [CrossRef]
42. Duan, H.; Feng, L.; Ma, R.; Zhang, Y.; Loiselle, S.A. Variability of particulate organic carbon in inland waters observed from MODIS Aqua imagery. *Environ. Res. Lett.* **2014**, *9*, 084011. [CrossRef]
43. Neil, C.; Cunningham, A.; McKee, D. Relationships between suspended mineral concentrations and red-waveband reflectances in moderately turbid shelf seas. *Remote Sens. Environ.* **2011**, *115*, 3719–3730. [CrossRef]
44. Volpe, V.; Silvestri, S.; Marani, M. Remote sensing retrieval of suspended sediment concentration in shallow waters. *Remote Sens. Environ.* **2011**, *115*, 44–54. [CrossRef]
45. Zhu, W.; Pang, S.; Chen, J.; Sun, N.; Huang, L.; Zhang, Y.; Zhang, Z.; He, S.; Cheng, Q. Spatiotemporal variations of total suspended matter in complex archipelagic regions using a sigmoid model and Landsat-8 imagery. *Reg. Stud. Mar. Sci.* **2020**, *36*, 101308. [CrossRef]
46. Alcântara, E.; Curtarelli, M.; Stech, J. Estimating total suspended matter using the particle backscattering coefficient: Results from the Itumbiara hydroelectric reservoir (Goiás State, Brazil). *Remote Sens. Lett.* **2016**, *7*, 397–406. [CrossRef]
47. DeLuca, N.M.; Zaitchik, B.F.; Curriero, F.C. Can Multispectral Information Improve Remotely Sensed Estimates of Total Suspended Solids? A Statistical Study in Chesapeake Bay. *Remote Sens.* **2018**, *10*, 1393. [CrossRef]
48. Chen, J.; Quan, W.; Cui, T.; Song, Q. Estimation of total suspended matter concentration from MODIS data using a neural network model in the China eastern coastal zone. *Estuar. Coast. Shelf Sci.* **2015**, *155*, 104–113. [CrossRef]
49. Che, T.; Li, X.; Jin, R. Monitoring the frozen duration of Qinghai Lake using satellite passive microwave remote sensing low frequency data. *Chin. Sci. Bull.* **2009**, *54*, 2294–2299. [CrossRef]
50. Qi, M.; Liu, S.; Yao, X.; Xie, F.; Gao, Y. Monitoring the Ice Phenology of Qinghai Lake from 1980 to 2018 Using Multisource Remote Sensing Data and Google Earth Engine. *Remote Sens.* **2020**, *12*, 2217. [CrossRef]
51. Cai, Y.; Ke, C.-Q.; Duan, Z. Monitoring ice variations in Qinghai Lake from 1979 to 2016 using passive microwave remote sensing data. *Sci. Total Environ.* **2017**, *607*, 120–131. [CrossRef]
52. Tang, L.; Duan, X.; Kong, F.; Zhang, F.; Zheng, Y.; Li, Z.; Mei, Y.; Zhao, Y.; Hu, S. Influences of climate change on area variation of Qinghai Lake on Qinghai-Tibetan Plateau since 1980s. *Sci. Rep.* **2018**, *8*, 7331. [CrossRef] [PubMed]
53. Zhang, G.; Duan, S. Lakes as sentinels of climate change on the Tibetan Plateau. *All Earth* **2021**, *33*, 161–165. [CrossRef]
54. Cao, Z.; Ma, R.; Duan, H.; Xue, K. Effects of broad bandwidth on the remote sensing of inland waters: Implications for high spatial resolution satellite data applications. *ISPRS J. Photogramm. Remote Sens.* **2019**, *153*, 110–122. [CrossRef]
55. Cao, Z.; Duan, H.; Shen, M.; Ma, R.; Xue, K.; Liu, D.; Xiao, Q. Using VIIRS/NPP and MODIS/Aqua data to provide a continuous record of suspended particulate matter in a highly turbid inland lake. *Int. J. Appl. Earth Obs.* **2018**, *64*, 256–265. [CrossRef]
56. Kutser, T.; Pierson, D.C.; Tranvik, L.J.; Reinart, A.; Sobek, S.; Kallio, K. Using Satellite Remote Sensing to Estimate the Colored Dissolved Organic Matter Absorption Coefficient in Lakes. *Ecosystems* **2005**, *8*, 709–720. [CrossRef]

57. Shi, K.; Zhang, Y.; Zhu, G.; Liu, X.; Zhou, Y.; Xu, H.; Qin, B.; Liu, G.; Li, Y. Long-term remote monitoring of total suspended matter concentration in Lake Taihu using 250 m MODIS-Aqua data. *Remote Sens. Environ.* **2015**, *164*, 43–56. [CrossRef]
58. Chen, S.; Huang, W.; Wang, H.; Li, D. Remote sensing assessment of sediment re-suspension during Hurricane Frances in Apalachicola Bay, USA. *Remote Sens. Environ.* **2009**, *113*, 2670–2681. [CrossRef]
59. Hou, X.; Feng, L.; Duan, H.; Chen, X.; Sun, D.; Shi, K. Fifteen-year monitoring of the turbidity dynamics in large lakes and reservoirs in the middle and lower basin of the Yangtze River, China. *Remote Sens. Environ.* **2017**, *190*, 107–121. [CrossRef]
60. Zheng, Z.; Ren, J.; Li, Y.; Huang, C.; Liu, G.; Du, C.; Lyu, H. Remote sensing of diffuse attenuation coefficient patterns from Landsat 8 OLI imagery of turbid inland waters: A case study of Dongting Lake. *Sci. Total Environ.* **2016**, *573*, 39–54. [CrossRef] [PubMed]
61. Shi, W.; Zhang, Y.; Wang, M. Deriving Total Suspended Matter Concentration from the Near-Infrared-Based Inherent Optical Properties over Turbid Waters: A Case Study in Lake Taihu. *Remote Sens.* **2018**, *10*, 333. [CrossRef]
62. Zhang, Y.; Shi, K.; Zhang, Y.; Moreno-Madrinan, M.J.; Li, Y.; Li, N. A semi-analytical model for estimating total suspended matter in highly turbid waters. *Opt. Express* **2018**, *26*, 34094–34112. [CrossRef] [PubMed]
63. Tarrant, P.; Amacher, J.A.; Neuer, S. Assessing the potential of Medium-Resolution Imaging Spectrometer (MERIS) and Moderate-Resolution Imaging Spectroradiometer (MODIS) data for monitoring total suspended matter in small and intermediate sized lakes and reservoirs. *Water Resour. Res.* **2010**, *46*, 1–7. [CrossRef]
64. Tassan, S. Local algorithms using SeaWiFS data for the retrieval of phytoplankton, pigments, suspended sediment, and yellow substance in coastal waters. *Appl. Opt.* **1994**, *33*, 2369–2378. [CrossRef] [PubMed]
65. Lu, H.; Yang, L.; Fan, Y.; Qian, X.; Liu, T. Novel simulation of aqueous total nitrogen and phosphorus concentrations in Taihu Lake with machine learning. *Environ. Res.* **2021**, *204*, 111940. [CrossRef] [PubMed]
66. Shang, W.; Jin, S.; He, Y.; Zhang, Y.; Li, J. Spatial–Temporal Variations of Total Nitrogen and Phosphorus in Poyang, Dongting and Taihu Lakes from Landsat-8 Data. *Water* **2021**, *13*, 1704. [CrossRef]
67. Wu, M.; Zhang, X.; Reis, S.; Ge, S.; Gu, B. Pollution controls in Lake Tai with the reduction of the watershed nitrogen footprint. *J. Clean. Prod.* **2021**, *332*, 130132. [CrossRef]
68. Xiong, J.; Lin, C.; Ma, R.; Cao, Z. Remote Sensing Estimation of Lake Total Phosphorus Concentration Based on MODIS: A Case Study of Lake Hongze. *Remote Sens.* **2019**, *11*, 2068. [CrossRef]
69. The Area Protection and Utilization Administration Bureau of Qinghai Province. Notice of the general office of Qinghai Provincial People's Government on printing and distributing the provisions on the functional allocation, internal institutions and staffing of Qinghai Lake Scenic Spot Protection and utilization administration. *Qinghai Political News* **2007**, 49. (In Chinese)
70. Liu, D.; Duan, H.; Loiselle, S.; Hu, C.; Zhang, G.; Li, J.; Yang, H.; Thompson, J.R.; Cao, Z.; Shen, M.; et al. Observations of water transparency in China's lakes from space. *Int. J. Appl. Earth Obs.* **2020**, *92*, 102187. [CrossRef]
71. Shen, M.; Duan, H.; Cao, Z.; Xue, K.; Qi, T.; Ma, J.; Liu, D.; Song, K.; Huang, C.; Song, X. Sentinel-3 OLCI observations of water clarity in large lakes in eastern China: Implications for SDG 6.3.2 evaluation. *Remote Sens. Environ.* **2020**, *247*, 111950. [CrossRef]
72. Xu, Y.; Qin, B.; Zhu, G.; Zhang, Y.; Shi, K.; Li, Y.; Shi, Y.; Chen, L. High Temporal Resolution Monitoring of Suspended Matter Changes from GOCI Measurements in Lake Taihu. *Remote Sens.* **2019**, *11*, 985. [CrossRef]
73. Cheng, L.; Yang, M.; Wang, X.; Wan, G. Spatial and Temporal Variations of Terrestrial Evapotranspiration in the Upper Taohe River Basin from 2001 to 2018 Based on MOD16 ET Data. *Adv. Meteorol.* **2020**, *2020*, 1–17. [CrossRef]
74. Zhang, T.; Chen, Y. Analysis of Dynamic Spatiotemporal Changes in Actual Evapotranspiration and Its Associated Factors in the Pearl River Basin Based on MOD16. *Water* **2017**, *9*, 832. [CrossRef]
75. Wang, Q.; Song, K.; Wen, Z.; Shang, Y.; Li, S.; Fang, C.; Du, J.; Zhao, F.; Liu, G. Long-term remote sensing of total suspended matter using Landsat series sensors in Hulun Lake, China. *Int. J. Remote Sens.* **2020**, *42*, 1379–1397. [CrossRef]
76. Tamm, T.; Nõges, T.; Järvet, A.; Bouraoui, F. Contributions of DOC from surface and groundflow into Lake Võrtsjärv (Estonia). *Hydrobiologia* **2008**, *599*, 213–220. [CrossRef]
77. Chang, B.; He, K.-N.; Li, R.-J.; Sheng, Z.-P.; Wang, H. Linkage of Climatic Factors and Human Activities with Water Level Fluctuations in Qinghai Lake in the Northeastern Tibetan Plateau, China. *Water* **2017**, *9*, 552. [CrossRef]